Inorganic Chemistry

Article

pubs.acs.org/IC

Role Played by Isopropyl Substituents in Stabilizing the Putative Triple Bond in Ar′EEAr′ [E = Si, Ge, Sn; Ar′ = C_6H_3-2,6-(C_6H_3-2,6-Pr^i_2)$_2$] and Ar*PbPbAr* [Ar* = C_6H_3-2,6-(C_6H_2-2,4,6-Pr^i_3)$_2$]

Issaka Seidu, Michael Seth, and Tom Ziegler*

Department of Chemistry, University of Calgary, 2500 University Dr. NW, Calgary, Alberta, Canada T2N 1N4

Supporting Information

ABSTRACT: A theoretical study of the bonding in ArEEAr (where E = Si, Ge, Sn, Pb; Ar = terphenyl ligand) revealed for the first time why bulky isopropyl substituents electronically are required in order to isolate stable ArEEAr species. This was accomplished by combining the natural orbitals for chemical valence (NOCV) method with the extended transition state (ETS) scheme. The NOCV−ETS analysis was based on two ArE fragments in their doublet ground state with the configuration $\sigma^2\pi^1$. For E = Si, Ge, and Sn, it revealed one π-bond perpendicular to the CEEC plane and two σ/π-type bonds in the plane, whereas the ArPbPbAr system was found to have a single σ bond with a C−Pb−Pb trans-bent angle close to 90°. While similar bonding pictures have been obtained in previous model studies with Ar = H and CH_3, the NOCV−ETS scheme was able to obtain quantitative estimates for the strength of various σ/π components without artificial truncations or twisting of the system. More importantly, NOCV−ETS analysis was able to show that the electronic influence of the isopropyl substituents on the σ/π components differs little from that found in a system where they are replaced by hydrogen. Instead, the favorable role of the isopropyl substituents is due to dispersive van der Waals attractions between Pr^i groups on aryl rings attached to different E atoms as well as hyperconjugation involving donation into σ^* orbitals on Pr^i. Dispersive interaction amounts to −27.5 kcal/mol (Si), −29.1 kcal/mol (Ge), −26.2 kcal/mol (Sn), and −44.0 kcal/mol (Pb). The larger dispersive stabilization for Pb reflects the fact that the longer Pb−Pb and Pb−C bonds sterically allow for more isopropyl groups with Ar = C_6H_3-2,6-(C_6H_2-2,4,6-Pr^i_3)$_2$. This is compared to the other elements where Ar = C_6H_3-2,6-(C_6H_3-2,6-Pr^i_2)$_2$. It is finally concluded from the analysis that real ArEEAr systems reveal little character of the EE bond in contrast to the findings of previous studies on model systems.

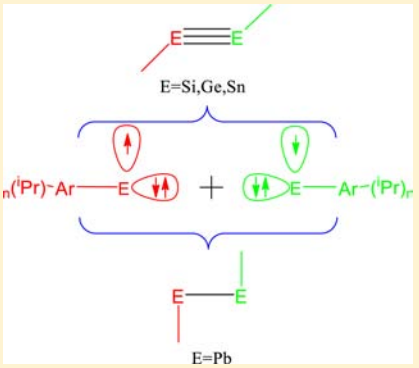

I. INTRODUCTION

Acetylene analogues of heavier group 14 elements (E = Si, Ge, Sn, Pb) have come under increasing scrutiny after the synthesis of the first homonuclear systems with the general formula ArEEAr (Ar = bulky aryl ligands) by Power et al.[1−5]

There have been several theoretical studies[6−29] on acetylene analogues both before and after the work by Power et al. Most of these investigations have been on model compounds such as E_2H_2[10,17] and E_2Me_2.[6,18−21] A remarkable exception is the work by Takagi and Nagase[29b] in which calculations on Ar*EEAr* [E = Si, Ge, Sn; Ar* = C_6H_3-2,6-(C_6H_2-2,4,6-Pr^i_3)$_2$] were presented simultaneously with or even prior to the isolation of similar compounds.

The studied E_2H_2 compound revealed that the linear structure is a second-order saddle point and the trans-bent geometry a local minimum or transition state[6] along the potential energy surface (PES).[22−25] The global minimum on the PES for E_2H_2 was found to be a structure in which the two E atoms are doubly bridged by two H atoms.[9−15,19−25]

The synthesis of the first homologous acetylene compound Ar*PbPbAr*[1] was followed shortly after by the isolation of Ar′GeGeAr′[2,5] and Ar′SnSnAr′.[3−6] All three species have a trans-bent structure with E−E−C bond angles of 94.3°, 125.2°, and 128.7° for E = Pb, Sn, and Ge, respectively. A diaryl Ar′SiSiAr′ compound for silicon is yet to be characterized. However, the synthesis of a silicon compound with the composition (R_2MeSi)SiSi($SiMeR_2$),[26,27] where R = Bu^t_3-Si and (R_2Pr^iSi)-SiSi($SiPr^iR_2$)[28] with R = $CH(Me_3Si)_2$, has been reported. The silicon compounds have a trans-bent geometry with an electronic structure[26−29] that is different from the triple-bonded carbon homologue (R_2MeSi)CC($SiMeR_2$) with a linear CSiSiC geometry.

It is the primary objective of the present study to assess whether Ar* is able electronically to stabilize the E−E bond either by electron donation from the isopropyl substituents (Pr^i) on the aryl rings or through dispersive van der Waals attraction between isopropyl groups on aryl rings attached to different E elements. We shall carry out this assessment by making use of the extended transition state (ETS) energy decomposition scheme[30−32] and the natural orbitals for chemical valence (NOCV) density decomposition approach,[33] as combined recently into the NOCV−ETS[34] scheme with van der Waals dispersion included according to the formulation of Grimme et al.[35] The pioneering theoretical studies on Ar*EEAr* [E = Si,

Received: December 18, 2012
Published: July 16, 2013

   dx.doi.org/10.1021/ic401149h | Inorg. Chem. 2013, 52, 8378−8388

Ge, Sn; Ar* = C_6H_3-2,6-(C_6H_2-2,4,6-Pr^i_3)$_2$] carried out previously[29a,b] by Takagi and Nagase employed a modest basis set. Further, no attempt was made to conduct a bonding analysis, and dispersion was neglected. Thus, while the authors could point to the possible steric role played by isopropyl, they were unable to assess in detail its possible electronic influence.

The conventional molecular orbital (MO) model used to describe the bonding in the trans-bent REER systems goes back some 25 years to the work by Tranquier and Malrieu[14a] as well as Carter and Goddard.[14b] It has recently been adopted in a lucid form by Takagi and Nagase[29a,b] for trans-bent systems of interest here. This frontier orbital description will also be the starting point for our description.

For the lighter elements with an REE angle of less than 180°, we have, as shown in **1**, a single out-of-plane π bond involving $\pi_{r(out)}$ and $\pi_{l(out)}$ as well as two in-plane bonding σ/π orbitals made up of $\pi_{r(in)}$, $\pi_{l(in)}$, L_r, and L_l. For the heavier members where the REE angle approaches 90°, the bonding scheme becomes as described in **2**, where the two in-plane $\pi_{r(in)}$ and $\pi_{l(in)}$ orbitals form a single σ-type bond. The relative strengths of the bonding components in **1** and **2** have been the matter of some discussion,[6,7,9] as has the identity of the element in the series E = Si, Ge, Sn, and Pb, at which the bonding picture crosses[6,7,9] from **1** to **2**. We shall for the first time give a quantitative comparison of the three bonding components in **1** for the real system based on energies rather than bond orders or other qualitative measures. The more restricted ETS method has previously been applied to model systems.[10] We shall further give a novel interpretation of the factors that cause the switch from **1** to **2**.

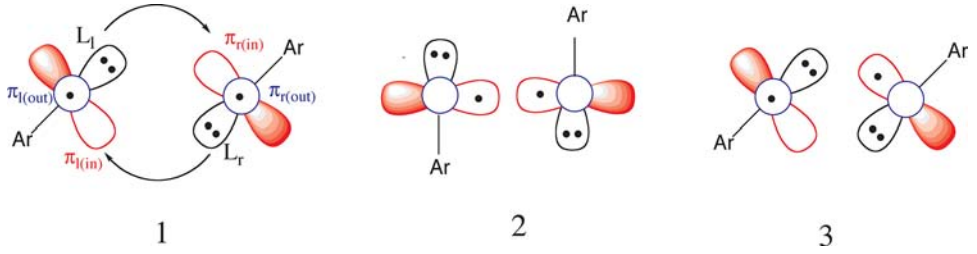

1 2 3

A final point is the degree of diradical character present in the bonding of REER. It has been claimed previously based on qualitative considerations[7] that the diractical character could be as high as 30% for the MeEEMe model systems. Here we shall demonstrate from more quantitative spin-flip calculations on the real systems that the diradical contributions such as **3** at the most amount to 5%.

II. THEORY

NOCV−ETS Scheme. In this scheme,[34] we consider a molecule AB of energy E_{AB} as formed from two fragments A^0 and B^0 with the energies E^0_A and E^0_B, respectively. The term ΔE_{AB} representing the formation energy of AB from A^0 and B^0 is defined as

$$\Delta E_{AB} = E_{AB} - E^0_A - E^0_B \tag{1}$$

The formation energy ΔE_{AB} can be decomposed[31,32] into five chemically meaningful components as

$$\Delta E_{AB} = \Delta E_{prep} + \Delta E_{elstat} + \Delta E_{Pauli} + \Delta E_{orb} + \Delta E_{disp} \tag{2}$$

The first component, ΔE_{prep}, is often referred to as the distortion or preparation energy. It is the energy required to distort and/or promote the two fragments from their equilibrium geometry to the structure that they will assume in the combined molecule. The second term, ΔE_{elstat}, corresponds to the electrostatic interaction energy between two distorted fragments as they are combined in the final molecule with the densities kept frozen. It is stabile for the neutral fragments studied in this work. The third contribution, ΔE_{Pauli}, is referred to as the Pauli repulsion term and originates from the destabilizing interaction between the occupied orbitals on the two fragments. The fourth component, ΔE_{orb}, is the orbital interaction energy. It is stabile and results from the interaction of occupied and virtual fragment orbitals. We finally have the stabilizing van der Waals dispersion interactions between the two fragments A and B.

The change in density due to orbital interactions can be written in terms of the orthogonalized fragment orbitals[34] (λ_μ; $\mu = 1, M$) on A and B as

$$\Delta\rho^{orb}(r) = \sum_{\mu}^{M}\sum_{\upsilon}^{M} \Delta P^{orb}_{\mu\upsilon}\lambda_\mu\lambda_\upsilon \tag{3}$$

where $\Delta P^{orb}_{\mu\upsilon}$ is the deformation density matrix. The orbital interaction energy can further be written as[34]

$$\Delta E_{orb} = \sum_{\mu}^{M}\sum_{\upsilon}^{M} \Delta P^{orb}_{\mu\upsilon}F^{TS}_{\mu\upsilon} = \mathrm{Tr}(\Delta P^{orb}F^{TS}) \tag{4}$$

Here $F^{TS}_{\mu\upsilon}$ is the Kohn−Sham (KS) matrix element between two fragment orbitals, λ_μ and λ_υ, with respect to a KS operator defined in terms of a density matrix halfway between that of the final molecule and the sum of the distorted fragments.[34] We can write ΔE_{orb} in a more compact form by first diagonalizing $\Delta P^{orb}_{\mu\upsilon}$ according to

$$\Delta P^{orb}C_i = \nu_i C_i \tag{5}$$

where the corresponding eigenvectors called natural orbitals for chemical valence, or NOCVs, are given by

$$\psi_j = \sum_k C_{jk}\lambda_k \tag{6}$$

The set of NOCVs can be[33,34] further divided into corresponding pairs (ψ_{-k}, ψ_k) with eigenvalues of the same magnitude, ν_k, but opposite signs. In the NOCV representation, the deformation density takes on the form

$$\Delta\rho^{orb}(r) = \sum_{k=1}^{M/2} \nu_k[-\Psi_{-k}{}^2(r) + \Psi_k{}^2(r)] = \sum_{k=1}^{M/2} \Delta\rho_k(r) \tag{7}$$

dx.doi.org/10.1021/ic401149h | Inorg. Chem. 2013, 52, 8378−8388

whereas ΔE_{orb} now is given as

$$\begin{aligned}\Delta E_{orb} &= \mathrm{Tr}(\Delta P^{orb} F^{TS}) \\ &= \mathrm{Tr}(C^{+}\Delta P^{orb} C C^{+} F^{TS} C) \\ &= \sum_{k=1}^{M/2} \nu_k [-F^{TS}_{-k,-k} + F^{TS}_{k,k}] \\ &= \sum_{k=1}^{M/2} \Delta E_k^{orb}\end{aligned} \tag{8}$$

where $F^{TS}_{-k,-k}$ and $F^{TS}_{k,k}$ are diagonal KS matrix elements over ψ_{-k} and ψ_k, respectively. Equations 6 and 7 relate to each change in density $\Delta\rho_k(r)$ the corresponding energy contribution ΔE_k^{orb}. Further $\Delta\rho_k(r)$ consists of density depletion $-\nu_k \Psi_{-k}{}^2(r)$ and the corresponding accumulation $\nu_k \Psi_k{}^2(r)$. In favorable cases,[34] different interactions such as σ, π, and δ bonding or σ donation and π back-donation can be identified with different k values and thus assessed individually, as we shall see shortly.

Spin-Flip Second-Order Constricted-Variational Density Functional Theory [SF-CV(2)-DFT] Method. The SF-CV(2)-DFT method[36] is based on a nondegenerate reference state that can be represented by a single KS determinant[37]

$$\Psi^0 = |\psi_1 \psi_2 \psi_3 \ldots \psi_i \psi_j \ldots \psi_n| \tag{9}$$

where $\{\psi_i(1); i = 1, \mathrm{occ}\}$ is a set of occupied orbitals and $\{\psi_a(1); a = 1, \mathrm{vir}\}$ the corresponding virtual orbitals with respect to that reference. The heavier acetylene congeners of group 14 elements are studied with a triplet reference state. Other microstates $\Psi_{i\to\bar{a}}$ are reached from the triplet reference through single orbital replacements $i \to \bar{a}$ and $\bar{i} \to \bar{a}$ involving spin flips. Here the superscript "bar" refers to an orbital of β spin. The corresponding singlet, triplet, and quartet states labeled I are subsequently determined as

$$\Psi^I = \sum_{\bar{a}i} U^I_{\bar{a}i} \Psi_{i\to\bar{a}} + \sum_{a\bar{i}} U^I_{a\bar{i}} \Psi_{\bar{i}\to a} \tag{10}$$

where the vector U^I is obtained from the eigenvalue equation

$$\mathbf{A}^{KS} \vec{U}^I = \lambda_I \vec{U}^I \tag{11}$$

and the eigenvalue λ_I represents the energy of state I relative to the triplet reference state.

The elements of the matrix $\mathbf{A}^{KS}$ are defined as

$$A^{KS}_{a\bar{i},b\bar{j}} = A^{KS}_{\bar{a}i,\bar{b}j} = \delta_{ab}\delta_{ij}(\varepsilon_{\bar{a}} - \varepsilon_i) + K^{KS}_{\bar{a}i,\bar{b}j} \tag{12}$$

In eq 10, $\varepsilon_{\bar{a}}$ and ε_i refer to reference state orbital energies. Further $K_{\bar{a}i,\bar{b}j} = K^{XC}_{\bar{a}i,\bar{b}j}$ where

$$K^{XC(HF)}_{\bar{a}i,\bar{b}j} = \int \bar{\phi}_a^*(1)\, \bar{\phi}_b(1)\, \frac{1}{r_{12}} \phi_i^*(2)\, \phi_j(2)\, \mathrm{d}\tau_1\, \mathrm{d}\tau_2 \tag{13}$$

for the Hartree–Fock (HF) exchange correlation and

$$K^{XC(KS)}_{\bar{a}i,\bar{b}j} = \frac{1}{2} \int \bar{\phi}_a^*(\bar{r}_1)\, \phi_i^*(\bar{r}_1)\, \bar{\phi}_b{}^*(\bar{r}_1)\, \phi_j\, {}^*(\bar{r}_1) \left[\left(\frac{1}{s^0} \left(\frac{\partial E^{KS}_{XC}}{\partial \rho_\alpha} - \frac{\partial E^{KS}_{XC}}{\partial \rho_\beta} \right) \right)_{(\rho^0, s^0)} \right] \mathrm{d}r_1 \tag{14}$$

for the local KS exchange correlation. In eqs 13 and 14, integration has already been carried out over spin. The expression for $K^{XC(KS)}_{\bar{a}i,\bar{b}j}$ derived by Wang and Ziegler[38−40] contains derivatives taken at the reference triplet electron charge and spin densities, ρ^0 and s^0, respectively. Practical evaluation of eq 14 has been discussed in previous applications of the SF-CV(2)-DFT method.[41−43]

III. COMPUTATIONAL DETAILS

Hamiltonian and Basis Set. All spin-flip calculations were performed with the unrestricted SF-CV(2)-DFT method employing the TZ2P[44] basis set implemented in the *ADF*[38] program. The functionals used include LDA-VWN,[45] BP86,[46,47] BLYP,[46,48] PBE,[49] B3LYP,[50] and BHLYP.[50] Relativistic effects were included at the scalar relativistic ZORA[51,52] level of approximation, whereas the dispersion term ΔE_{disp} of eq 2 was described by the scheme from Grimme et al.[35]

Molecular Models. We studied four of the heavier acetylene congeners of group 14. Crystal structures were available for Ge,[2] Sn,[1] and Pb.[6] The Si compound was optimized at the BP86 level. All of the compounds are homonuclear and have a trans-bent geometry with the general formula Ar′EEAr′ [E = Si, Ge, Sn; Ar′ = C_6H_3-2,6-(C_6H_2-2,6-Pr^i_3)$_2$] and Ar*PbPbAr* [Ar* = C_6H_3-2,6-(C_6H_2-2,4,6-Pr^i_3)$_2$]. The structures are shown in Figure 1.

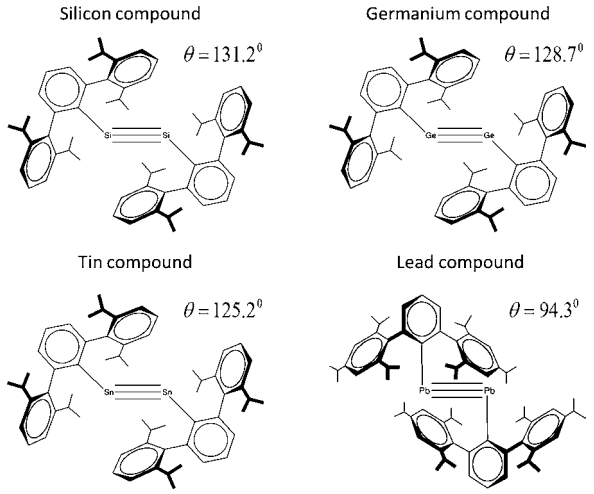

Figure 1. Structures of the four studied compounds from Si to Pb. Also given in each case is the CEE angle θ.

IV. RESULTS AND DISCUSSION

Fragment Orbitals. In NOCV analysis, we consider in line with **1** the compound ArEEAr as formed from two ArE units. Each has two π and one σ orbitals of importance for the E–E bond formation, as shown in Figure 2. The figure displays the fragment orbitals for Si and Pb with their corresponding energies as well as the levels for Ge and Sn. The fragment orbitals of the Ge and Sn compounds are similar to those of the Si system and are therefore omitted.

The π set on each fragment is not degenerate because of the Ar ligands. It consists of π^y, which is perpendicular to the CEEC plane in the overall ArEEAr molecule, and π^x, situated in the CEEC plane (Figure 2). A study of ArE (E = Si, Ge, Sn, and Pb) revealed a doublet ground state with the valence configuration $\sigma^2(\pi^y)^1(\pi^x)^0$ for E = Si, Ge, and Sn compared to $\sigma^2(\pi^x)^1(\pi^y)^0$ for E = Pb. The doublets with the opposite occupation of the π orbitals were 12.6 kcal/mol (Si), 14.2 kcal/mol (Ge), 20.4 kcal/mol (Sn), and 16.2 kcal/mol (Pb) higher in energy. The different preferences for occupation of the π orbitals between E = Si, Ge, and Sb, on the one hand, and E = Pb, on the other hand, must reflect that Ar in the cases of E = Si, Ge, and Sb is C_6H_3-2,6-(C_6H_3-2,6-Pr^i_2)$_2$ compared to C_6H_3-2,6-(C_6H_2-2,4,6-Pr^i_3)$_2$

dx.doi.org/10.1021/ic401149h | Inorg. Chem. 2013, 52, 8378–8388

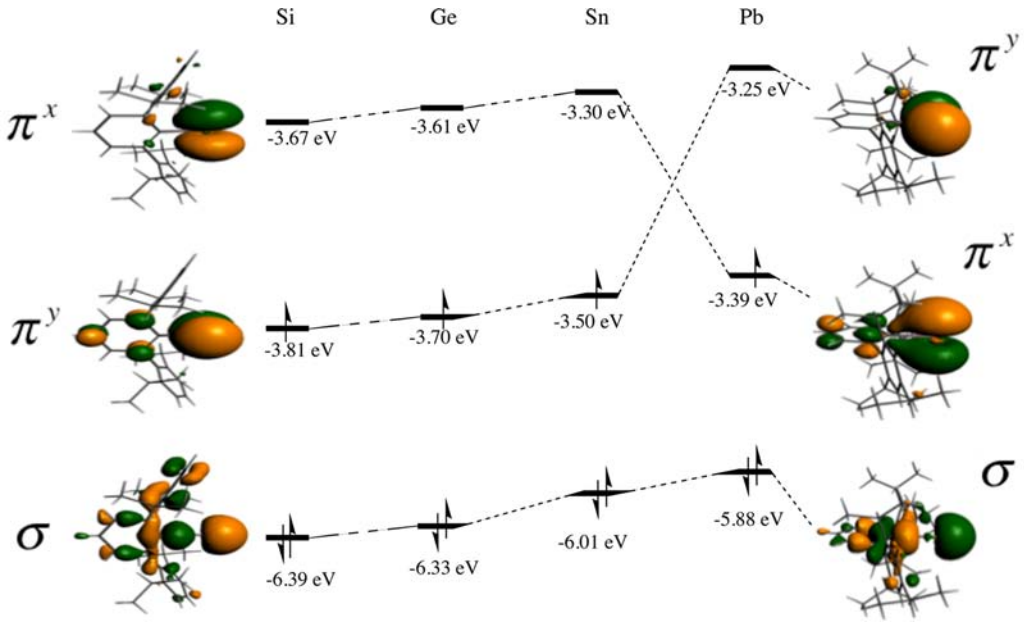

Figure 2. Fragment orbitals of ArE for E = Si and Pb with corresponding energy levels for E = Si, Ge, Sn, and Pb.

for E = Pb. However, we have not pursued this question further. The quartet state with the valence configuration $\sigma^1(\pi^y)^1(\pi^x)^1$ was found to be 50−70 kcal/mol higher in energy than the doublet ground state depending on E.

For all four elements, the σ orbital is of lower energy than the two π components by some 2.5 eV because of a sizable contribution from the *n*s orbital ($n = 3, 6$) on E. This is why the σ level is occupied by two electrons in the fragment ground state. We shall in the following analyze the bonding in ArEEAr in terms of the two doublet fragments in their electronic ground state.

We illustrate in Figure 3 linear combinations of equivalent σ and π^x orbitals on the two fragments as a function of the

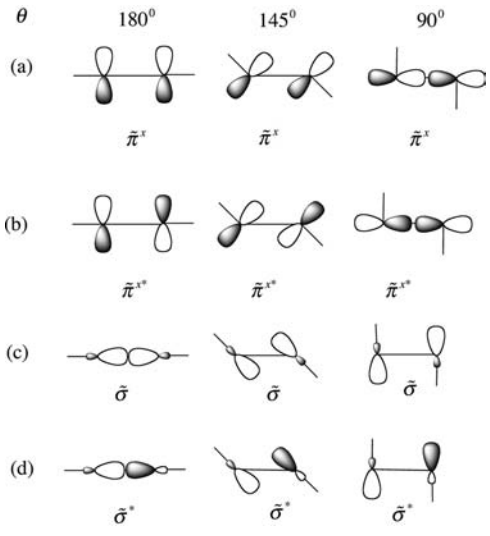

Figure 3. Combinations of σ and π fragment orbitals as a function of the trans-bending angle θ.

trans-bent ∠CEE angle θ. It is important to note that the in-phase π^x combination $\tilde{\pi}^x$ goes from being π-bonding at 180° to σ-antibonding at 90°, whereas the out-of-phase π^x combination $\tilde{\pi}^{x*}$ starts out as π-antibonding at θ = 180° and ends up as σ-bonding at 90°. Around θ = 145°, $\tilde{\pi}^{x*}$ is already bonding, whereas $\tilde{\pi}^x$ is antibonding. For the σ component, the in-phase combination $\tilde{\sigma}$ is σ-bonding at θ = 180° and mildly π-antibonding at 90°, whereas the out-of-phase combination $\tilde{\sigma}^*$ is σ-antibonding at θ = 180° and mildly π-bonding at 90°. Not shown in Figure 3 are the bonding and antibonding combinations $\tilde{\pi}^y$ and $\tilde{\pi}^{y*}$, respectively, of the out-of-plane π^y fragment orbitals. They do not change bonding character with θ.

MOs. The frontier MOs are shown in Figure 4 for the trans-bent Si compound with θ = 131° to the left. The orbital of lowest energy is made up of an in-phase combination of $\tilde{\pi}^{x*}$and $\tilde{\sigma}$ from Figure 3 with a slight majority contribution from $\tilde{\sigma}$. It is denoted as σ_{EE} because of its strong σ-bonding character. The second lowest occupied MO is primarily $\tilde{\sigma}^*$ and labeled as $\sigma_{EE}{}^*$, although it mostly is π-bonding as discussed above. The occupied orbital of highest energy, named π^y_{EE}, is a bonding combination of the fragment π^y orbitals ($\tilde{\pi}^y$) situated perpendicular to the CEEC plane. The unoccupied orbital of lowest energy, π^x_{EE}, is an out-of-phase combination of $\tilde{\pi}^{x*}$ and $\tilde{\sigma}$, with the largest contribution from $\tilde{\pi}^{x*}$. The occupation and relative energies of the four frontier orbitals for E = Ge and Sn are also shown in Figure 4. They differ little from E = Si; thus, their composition is not shown in Figure 4. We find for trans-bent Ar′SiSiAr′ that the gross population of the three orbitals on each fragment in the overall complex is $(\sigma)^{1.64}(\pi^x)^{0.46}(\pi^y)^{0.94}$ compared to $(\sigma)^2(\pi^x)^0(\pi^y)^1$ for a free fragment. Similar gross populations were obtained for E = Ge and Sn.

The MOs of the trans-bent Pb compound with θ = 94.3° are also shown in Figure 4. We see that $\sigma_{EE}{}^*$ and σ_{EE} are of lowest energy. They are almost solely made up of $\tilde{\sigma}^*$ and $\tilde{\sigma}$, respectively, with the first appearing as π-bonding and the second as π-antibonding, in accordance with the discussion above. As the HOMO, we now find the in-plane π orbital π^x_{EE} made up of $\tilde{\pi}^{x*}$, whereas the LUMO has become π^y_{EE}. It would appear that a longer E−E distance and smaller C−E−E angle make the σ-type overlap between the two π^x fragments in π^x_{EE} more stabile than the π-type overlap in π^y_{EE} with the result that π^{x*}_{EE} now is of lower energy than π^y_{EE} and occupied, whereas π^y_{EE} has become the LUMO. Frenking and co-workers found a similar switchover for

dx.doi.org/10.1021/ic401149h | *Inorg. Chem.* 2013, 52, 8378−8388

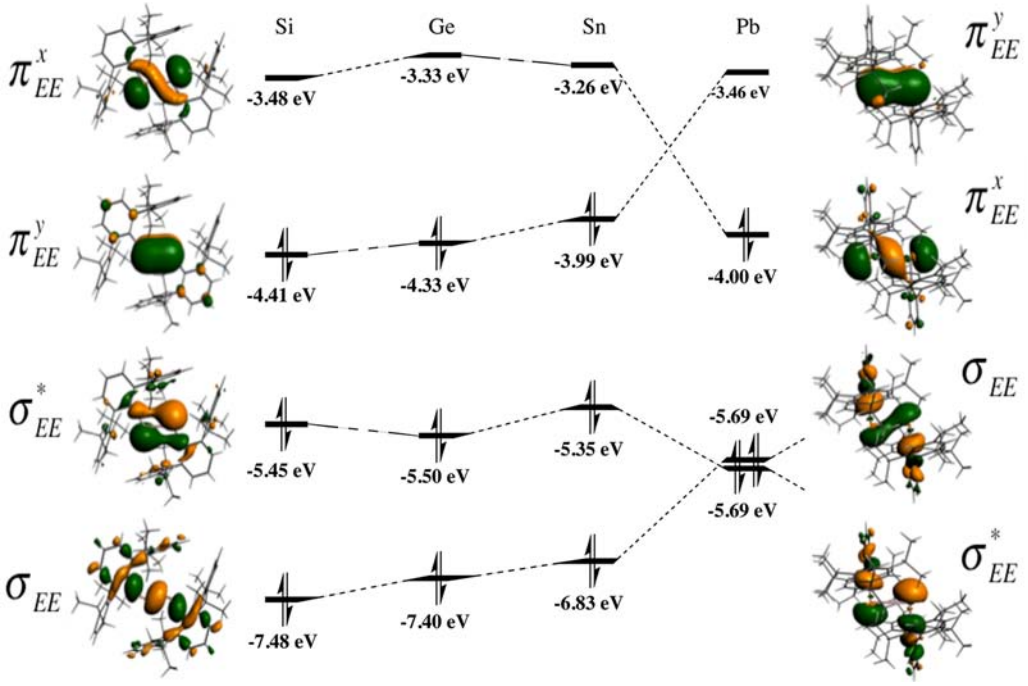

Figure 4. MOs of trans-bent ArEEAr for E = Si and Pb as well as the corresponding orbital energies for E = Si, Ge, Sn, and Pb.

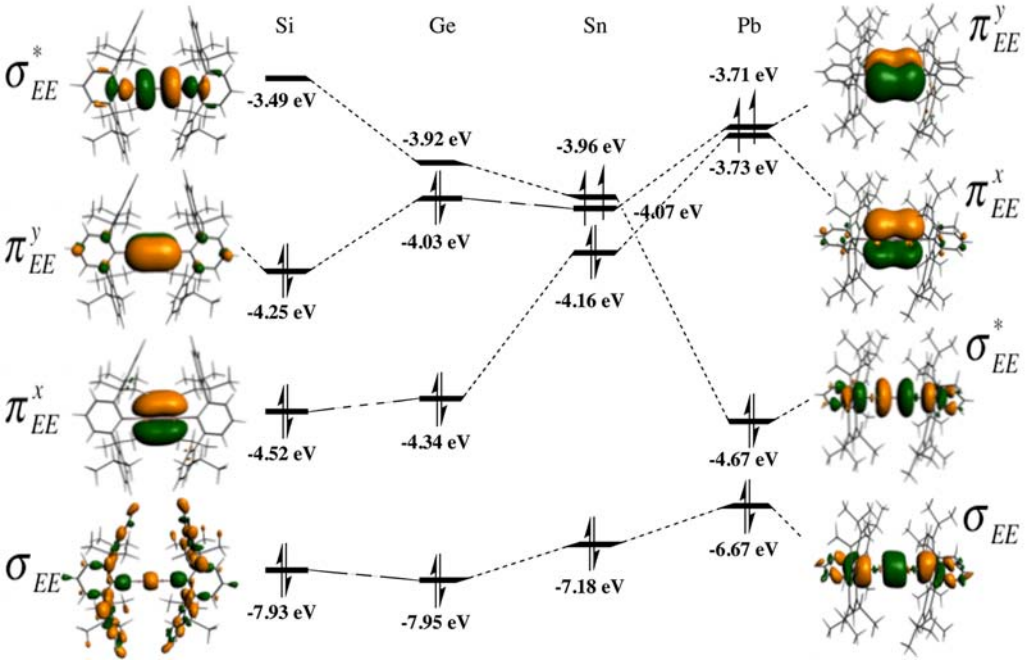

Figure 5. MOs of linear ArEEAr for E = Si and Pb and the corresponding orbital energies for E = Si, Ge, Sn, and Pb.

the HEEH model compounds.[9] However, as far as we are aware, this is the first rationale given of the crossover in terms of the decreasing bonding overlap in $\tilde{\pi}^y$ compared to $\tilde{\pi}^{x*}$ as the E−E bond distance increases. Frenking[9] and others[7] have interpreted the crossover as being caused by an increasing stability of the doublet compared to the quartet in ER toward heavier congeners of E. Certainly, this might be a contributing factor as well. The gross population of each Ar*Pb fragment in trans-bent Ar*PbPbAr* is $(\sigma)^{1.92}(\pi^x)^{1.04}(\pi^y)^{0.06}$ compared to $(\sigma)^2(\pi^x)^1(\pi^y)^0$ for the free ligand.

Figure 5 depicts the MOs obtained for the linear Si and Pb compounds with their corresponding energies as well as the energy levels of the Ge and Sn compounds. The MOs of the Si compound are comprised of two π-bonding and one σ-bonding combinations. Lowest in energy is $\sigma_{EE}(\tilde{\sigma})$ followed by $\pi^x_{EE}(\tilde{\pi}^x)$ and $\pi^y_{EE}(\tilde{\pi}^y)$. The lowest-lying empty orbital is $\sigma_{EE}{}^*(\tilde{\sigma}^*)$. As shown in Figure 5, the same occupation and ordering is found for the Ge and Sn compounds, although the gap between π^y_{EE} and $\sigma_{EE}{}^*$ decreases. For the linear Pb compound, we find that $\sigma_{EE}{}^*$ now becomes occupied, whereas π^y_{EE} takes on the role of the

dx.doi.org/10.1021/ic401149h | Inorg. Chem. 2013, 52, 8378−8388

LUMO. Thus, for E = Si, Ge, and Sn, the σ_{EE}* orbital is empty because of the strongly antibonding σ overlap in the linear ArEEAr molecule. This is in spite of the fact that the constituting σ fragment orbitals are more stable than the corresponding π^x and π^y components. Instead, the HOMO is made up of π^y_{EE}, where the lower stability of π^y compared to σ is compensated for by a bonding π overlap. Through the series E = Si, Ge, Sn, and Pb, the stabilizing π overlap is reduced and the antibonding σ overlap diminished. As a result, σ_{EE}* first approaches π^x_{EE} and π^y_{EE} and than dips below the two π orbitals at E = Pb. The gross populations in linear ArEEAr are $(\sigma)^{1.24}(\pi^x)^{0.98}(\pi^y)^{0.94}$ for E = Si with similar values for E = Ge and Sn and $(\sigma)^{1.86}(\pi^x)^{0.94}(\pi^y)^0$ for E = Pb.

NOCV−ETS Analysis of Trans-Bent Compounds Based on ArE Fragments with a Doublet State. Starting with the E−E bond formed from two doublet ArE fragments of opposite spin polarization (ArE↑↓↑ and ↓↑↓EAr), we provide the ΔE_{EE} bond energy decomposition according to (2) in Table 1 for

Table 1. ETS[c] Analysis for Trans-Bent Ar′SiSiAr′ Carried Out with Different Functionals (Energies in kcal/mol)

functional	ΔE_{Pauli}	ΔE_{elstat}	ΔE_{steric} [a]	ΔE_{orb}	ΔE_{disp}	ΔE_{int} [b]
LDA	117.2	−70.1	47.1	−129.6	−17.8	−100.2
BP86	141.4	−69.6	71.8	−123.3	−27.5	−79.0
B3LYP	149.6	−72.3	77.3	−119.8	−24.7	−67.2
BHLYP	153.8	−77.0	76.8	−121.1	−17.8	−62.0

[a]Steric interaction energy, $\Delta E_{steric} = \Delta E_{Pauli} + \Delta E_{elstat}$. [b]Fragment interaction energy, $\Delta E_{int} = \Delta E_{steric} + \Delta E_{orb} + \Delta E_{disp}$. [c]Based on doublet fragments.

E = Si using four different functionals, LDA, BP86, B3LYP, and BHLYP. As expected, the Pauli term ΔE_{Pauli} is large and positive. It is significantly less repulsive for LDA with 117.2 kcal/mol than for the other three functionals with 141.4 kcal/mol (BP86), 149.6 kcal/mol (B3LYP), and 153.8 kcal/mol (BHLYP), respectively. The Pauli contribution is, in part, canceled by the numerically large and attractive (negative) electrostatic contribution that is quite similar for the different functionals. It is customary[34,53] to combine the numerically large ΔE_{elstat} and ΔE_{Pauli} contributions into the smaller steric interaction energy

$$\Delta E_{steric} = \Delta E_{Pauli} + \Delta E_{elstat} \quad (15)$$

The steric term represents the total destabilizing interaction of the occupied orbitals on the two fragments. It is usually positive when we, as in the case here, are dealing with neutral fragments and ranges from 47.1 kcal/mol (LDA) to 77.3 kcal/mol (B3LYP) (Table 1). The fact that LDA, in general, underestimates Pauli repulsion is the primary reason why this functional most often overestimates bond energies.

The van der Waals dispersion ΔE_{disp} is stabile and far from negligible, with contributions between −17.8 kcal/mol (LDA) and −27.8 kcal/mol (BP86) depending on the functional (Table 1). A large part of ΔE_{disp} comes from the van der Waals interaction between Pr^i groups on different fragments. Stable ArEEAr compounds often contain Pr^i groups, and it is thus clear from our analysis that one of the roles played by Pr^i is to stabilize the ArE dimer through ΔE_{disp}. This contribution has previously been neglected in theoretical studies of ArEEAr.[29]

The orbital interaction ΔE_{orb} is numerically large and stabile (Table 1). It is further quite similar for the four functionals and makes up the leading term in the expression for the interaction energy ΔE_{int} between the two distorted doublet fragments given by

$$\Delta E_{int} = \Delta E_{steric} + \Delta E_{disp} + \Delta E_{orb} \quad (16)$$

It is important to note that LDA has the most stabilizing interaction energy with ΔE_{int} = −100.2 kcal/mol as a result of the weaker steric repulsion. On the other hand, for the other functionals, ΔE_{int} decreases gradually in absolute terms as −79.0 kcal/mol (BP86), −67.2 kcal/mol (B3LYP), and −62.0 (BHLYP).

Table 2 provides an ETS analysis of the E−E bond in the real trans-bent ArEEAr systems for E = Si, Ge, Sn, and Pb based on the BP86 functional. It is clear from the table that the steric interaction energy ΔE_{steric} follows the trend Si ∼ Ge > Sn > Pb, as the E−E distance increases on going from Ge to Pb. A similar trend is observed for $-\Delta E_{orb}$. One would thus expect from eq 16 that $-\Delta E_{int}$ should decline as Si ∼ Ge > Sn > Pb through the series toward the heavier congener. We see instead the trend Si ∼ Ge > Sn < Pb because $-\Delta E_{int}$ is larger for Pb than for Sn. This reversal is due to ΔE_{disp}, which is more stabile for E = Pd than for any of the other elements as a result of the larger number of Pr^i groups on each Ar*Pb fragment [Ar* = C_6H_3-2,6-(C_6H_2-2,4,6-Pr^i_3)$_2$] compared to Ar′E [E = Si, Ge, Sn; Ar′ = C_6H_3-2,6-(C_6H_3-2,6-Pr^i_2)$_2$]. It might appear counterintuitive that the steric interaction decreases with the core size of E. However, this is compensated for by a longer E−E distance. Also, the longer E−E bond diminishes the steric interaction between the two Ar groups for the real systems.

We can probe the influence of the isopropyl groups further by replacing all of them in the real systems with H atoms and reoptimizing the C−H distances while keeping the rest of the framework frozen. It follows from Table 3 that Pr^i removal

Table 3. ETS[d,e] Analysis of the Trans-Bent[c] ArEEAr Model Systems Carried Out with the BP86 Functional

ArEEAr	ΔE_{Pauli}	ΔE_{elstat}	ΔE_{steric} [a]	ΔE_{orb}	ΔE_{disp}	ΔE_{int} [b]
Si[c]	131.8	−65.2	66.6	−116.0	−14.6	−64.0
Ge[c]	158.7	−86.8	71.9	−113.6	−15.7	−57.4
Sn[c]	114.4	−66.5	47.9	−74.9	−15.0	−42.0
Pb[c]	84.8	−65.2	19.6	−51.0	−9.8	−41.2

[a]Steric interaction energy, $\Delta E_{steric} = \Delta E_{Pauli} + \Delta E_{elstat}$. [b]Total Interaction energy, $\Delta E_{int} = \Delta E_{steric} + \Delta E_{orb} + \Delta E_{disp}$. [c]Ar = C_6H_3-2,6-(C_6H_5)$_2$. [d]Based on doublet fragments. [e]Energies in kcal/mol.

Table 2. ETS[e,g] Analysis of the Trans-Bent Compounds Carried Out with the BP86 Functional for the Real Systems

ArEEAr	ΔE_{Pauli}	ΔE_{elstat}	ΔE_{steric} [a]	ΔE_{orb}	ΔE_{disp}	ΔE_{int} [b]	ΔE_{prep}	ΔE_{EE} [f]
Si[c]	141.4	−69.6	71.8	−123.3	−27.5	−79.0	41.2	−37.8
Ge[c]	168.7	−91.8	76.9	−121.6	−29.1	−73.7	43.9	−29.8
Sn[c]	122.2	−71.3	50.9	−81.4	−26.2	−56.7	28.0	−28.7
Pb[d]	121.5	−84.6	37.0	−71.7	−44.0	−78.7	13.7	−65.0

[a]Steric interaction energy, $\Delta E_{steric} = \Delta E_{Pauli} + \Delta E_{elstat}$. [b]Total Interaction energy, $\Delta E_{int} = \Delta E_{steric} + \Delta E_{orb} + \Delta E_{disp}$. [c]Ar′ = C_6H_3-2,6-(C_6H_3-2,6-iPr_2)$_2$. [d]Ar* = C_6H_3-2,6-(C_6H_2-2,4,6-iPr_3)$_2$. [e]Based on doublet fragments. [f]$\Delta E_{EE} = \Delta E_{int} + \Delta E_{prep}$. [g]Energies in kcal/mol.

dx.doi.org/10.1021/ic401149h | Inorg. Chem. 2013, 52, 8378−8388

reduces the steric repulsion ΔE_{steric}, as one might expect. On the other hand, there is a substantial reduction in the dispersive stabilization ΔE_{disp} and a somewhat smaller numerical decrease in the orbital interaction energy ΔE_{orb}. We shall discuss the decrease in $-\Delta E_{orb}$ shortly. Here we note that the net effect of Pr^i removal is to reduce $-\Delta E_{int}$ in absolute terms through the loss of dispersion and thus reduce the strength of the E−E bond.

In order to calculate the total bond energy ΔE_{EE} between the two ArE monomers according to

$$\Delta E_{EE} = \Delta E_{int} + \Delta E_{prep} \tag{17}$$

we need as well the preparation term ΔE_{prep}. In the current case, where we are using the fragments in their electronic ground state, this term represents the energy required to change the two fragments from the doublet ground state to the distorted doublet state in the overall molecule. The term ΔE_{prep} decreases from E = Ge to E = Pb (Table 2). We observed a lower preparation term for E = Si compared to E = Ge. The total bond energy, ΔE_{EE}, decreased in absolute terms from E = Si to E = Sn and increased again toward E = Pb with the numerically largest value. This is indicative of the strong dispersive stabilization for E = Pb. Without ΔE_{disp}, the bond energy $-\Delta E_{EE}$ would decrease from Si to Pb, as found by Takagi and Nagase[29b] in their pioneering study where ΔE_{disp} was neglected.

In Table 4, we provide NOCV decomposition of ΔE_{orb} based on the BP86 functional for E = Si, Ge, Sn, and Pb according to

Table 4. NOCV[c] Contributions[a] to ΔE_{orb}[b] for the Trans-Bent Compounds Carried Out with the BP86 Functional for the Real Systems

compound	$\Delta E^{\pi^y}_{orb}$ [b]	$\Delta E^{\sigma-\pi*}_{orb}$	$\Delta E^{\sigma-\pi*}_{orb}$	$\Delta E^{\pi^x*}_{orb}$	ΔE^{rest}_{orb}
Si[d]	−32.4	−36.6	−38.2		−13.4
Ge[d]	−33.1	−35.7	−35.6		−14.2
Sn[d]	−23.1	−19.2	−25.1		−11.8
Pb[e]				−45.4	−24.7

[a]See Figures 6 and 8. [b]$\Delta E_{orb} = \Delta E^{\pi^y}_{orb} + \Delta E^{\sigma*-\pi}_{orb} + \Delta E^{\sigma-\pi*}_{orb} + \Delta E^{rest}_{orb}$ for E = Si, Ge, and Sn. [c]Based on doublet fragments. [d]Ar′ = C_6H_3-2,6-(C_6H_3-2,6-iPr$_2$)$_2$. [e]Ar* = C_6H_3-2,6-(C_6H_2-2,4,6-iPr$_3$)$_2$. [f]Energies in kcal/mol.

$$\Delta E_{orb} = \Delta E^{\pi^y}_{orb} + \Delta E^{\sigma-\pi^*}_{orb} + \Delta E^{\sigma^*-\pi}_{orb} + \Delta E^{rest}_{orb} \tag{18}$$

The change in density $\Delta\rho_k$ corresponding to the three major contributions $\Delta E^{\pi^y}_{orb}$, $\Delta E^{\sigma-\pi*}_{orb}$, and $\Delta E^{\sigma*-\pi}_{orb}$ are depicted in Figure 6 for E = Si. The analysis is based on two doublet fragments each with the electronic configuration $\sigma^2(\pi^y)^1(\pi^x)^0$. We provide in addition for each $\Delta\rho_k$ in Figure 7 the corresponding pair of NOCV orbitals (ψ_{-k}, ψ_k) contributing to $\Delta\rho_k$ according to eq 7.

Figure 6a illustrates the π^y bond formed by an outflow of α-electron density ($\Delta\rho^{\pi^y,\alpha}_{orb}$) from the occupied fragment π^y orbital on the left side (orange) and an inflow to the empty π^y orbital on the right side (green). The corresponding NOCVs are shown in Figure 7a. Here Ψ^{α}_{-1} represents the orthogonalized occupied fragment π^y orbital on the left side and Ψ^{α}_{1} the empty π^y orbital on the right side. The corresponding charge flow of the β-electron density in the opposite direction $\Delta\rho^{\pi^y,\beta}_{orb}$ is omitted from Figure 6. However, Figure 6a contains the sum $\Delta\rho^{\pi^y}_{orb}$. It follows from Figure 6a and Table 6 that the contribution to ΔE_{orb} from $\Delta\rho^{\pi^y}_{orb}$ amounts to $\Delta E^{\pi^y}_{orb}$ = −32.4 kcal/mol. The term $\Delta E^{\pi^y}_{orb}$ is obviously related to the formation of the π^y_{EE} orbital, which is the HOMO in Figure 4.

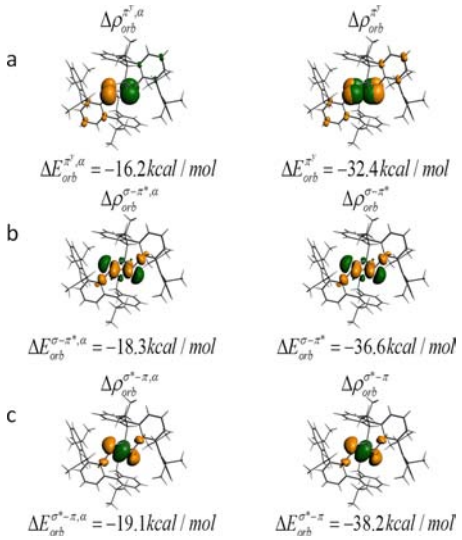

Figure 6. NOCV deformation densities for the trans-bent Si compound based on doublet fragments. (a) Contours of the π^y-NOCV deformation density with the corresponding energy contributions. The contour values are 0.003 au. (b) Contours of the σ^*/π-NOCV deformation density with the corresponding energy contributions. The contour values are 0.003. (c) Contours of the σ/π^*-NOCV deformation density with the corresponding energy contributions. The contour values are 0.003. Green represents positive contours and orange negative contours.

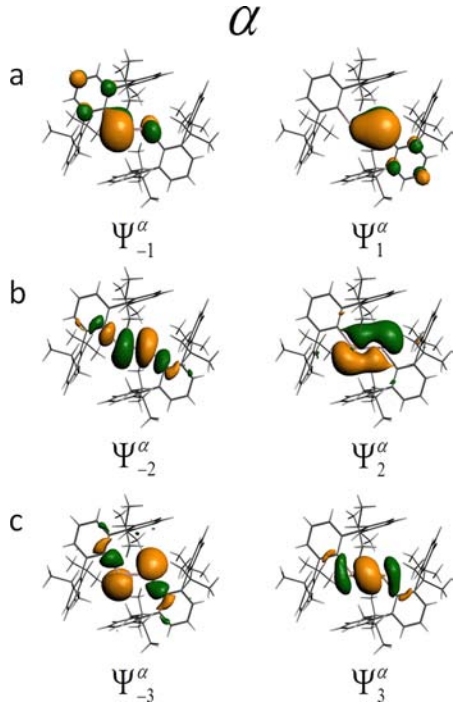

Figure 7. NOCVs for the three major contributions to $\Delta\rho_{orb}$ for trans-bent ArSiSiAr based on doublet fragments.

Figure 6b displays the relocation of charge $\Delta\rho^{\sigma*-\pi,\alpha}_{orb}$ from the $\tilde{\sigma}^*$ combination depicted in Figure 7b as Ψ^{α}_{-2} to $\tilde{\pi}^x$ depicted in Figure 7b as Ψ^{α}_{2}. The figure illustrates both the α-density relocation $\Delta\rho^{\sigma*-\pi,\alpha}_{orb}$ and the total change $\Delta\rho^{\sigma*-\pi}_{orb} = \Delta\rho^{\sigma*-\pi,\alpha}_{orb} + \Delta\rho^{\sigma*-\pi,\beta}_{orb}$. The orbital stabilization due to $\Delta\rho^{\sigma*-\pi}_{orb}$ amounts to $\Delta E^{\sigma*-\pi}_{orb}$ = −36.6 kcal/mol (Figure 6b). It is obvious that $\Delta\rho^{\sigma*-\pi}_{orb}$ is associated with the formation of the σ_{EE}* orbital in Figure 4.

dx.doi.org/10.1021/ic401149h | Inorg. Chem. 2013, 52, 8378−8388

Figure 6c depicts transfer of the α-electron density ($\Delta\rho_{orb}^{\sigma-\pi*}$) from $\tilde{\sigma}$ shown in Figure 7c as Ψ_{-3}^{α} to $\tilde{\pi}^{x*}$ given in Figure 7c as Ψ_{3}^{α}. Also presented is $\Delta\rho_{orb}^{\sigma-\pi*} = \Delta\rho_{orb}^{\sigma-\pi*,\alpha} + \Delta\rho_{orb}^{\sigma-\pi*,\beta}$. It is clear that $\Delta\rho_{orb}^{\sigma-\pi*}$ corresponds to the formation of σ_{EE} in Figure 4. The stabilization corresponding to $\Delta\rho_{orb}^{\sigma-\pi*}$ is $\Delta E_{orb}^{\sigma-\pi*} = -38.2$ kcal/mol. Finally shown in Table 4 is $\Delta E_{orb}^{rest} = -13.4$ kcal/mol. It represents primarily charge polarization on the aryl rings and is not shown in Figure 6.

Going next from E = Si to E = Ge and Sn leads to deformation densities $\Delta\rho_{orb}^{\pi^{y}}$, $\Delta\rho_{orb}^{\sigma*-\pi}$, and $\Delta\rho_{orb}^{\sigma-\pi*}$ that are qualitatively similar from one element to the next. Further, the corresponding energy contributions $\Delta E_{orb}^{\pi^{y}}$, $\Delta E_{orb}^{\sigma*-\pi}$, and $\Delta E_{orb}^{\sigma-\pi*}$ are seen to be comparable for E = Si and Ge before they decline in absolute terms for E = Sn as the E−E distance increases. In summary, our NOCV analysis indicates that trans-bent ArEEAr for E = Si, Ge, and Sn has a triple bond consisting of an out-of-plane π bond and two in-plane bonds. One in-plane bond is made up of $\tilde{\sigma}^*$ (65%) and $\tilde{\pi}^{x}$ (35%) from Figure 3 and the other of $\tilde{\sigma}$ (70%) and $\tilde{\pi}^{x*}$ (30%). For a given E, all three bond components have about the same strength (Table 4).

For Ar*PbPbAr*, we find only one important bond component corresponding to $\Delta\rho_{orb}^{\pi^{x}}$ (Figure 8). It represents

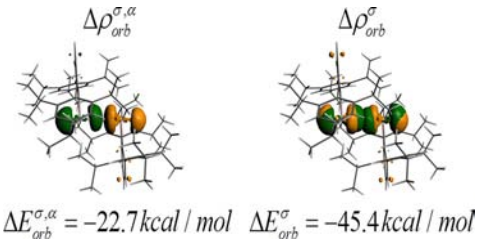

Figure 8. NOCV deformation densities for the trans-bent Pb compound based on doublet fragments. Contours of the σ-NOCV deformation density with the corresponding energy contributions. The contour values are 0.002 au. Green represents positive contours and orange negative contours.

transfer of the α density from an occupied in-plane π^{x} orbital on one fragment to an empty π^{x} orbital on the other fragment, $\Delta\rho_{orb}^{\pi^{x},\alpha}$, as well as transfer of the β density in the opposite direction, $\Delta\rho_{orb}^{\pi^{x},\alpha}$ (Figure 8). The total contribution to ΔE_{orb} from $\Delta\rho_{orb}^{\pi^{x}}$ is $\Delta E_{orb}^{\pi^{x}} = -45.4$ kcal/mol. Thus, in Ar*PbPbAr*, we have only a single bond. This is consistent with the MO diagram in Figure 4, where both σ_{EE} and σ_{EE}* are occupied and made up solely of $\tilde{\sigma}$ and $\tilde{\sigma}$*, respectively. Thus, combined they do not contribute to the bond order. The only contribution comes from π_{EE}^{x*} made up of $\tilde{\pi}^{x*}$, which at the trans-bent angle of 94.3° forms a σ-type bond, as illustrated in Figures 3 and 4. With a bond order of 1, one might have expected the E−E link to be weaker for E = Pb than for the three other elements with formal triple bonds. Indeed, ΔE_{orb} is smallest for E = Pb in absolute terms. However, this is compensated for by a modest steric interaction and a very favorable van der Waals attraction ΔE_{disp} (Table 4). As a result, $-\Delta E_{int}$ for Pb is comparable to that for Si and larger than $-\Delta E_{int}$ for E = Ge and Sn (Table 4). We have also calculated the NOCV contributions to ΔE_{orb} for the model systems ArEEAr with Ar = C_6H_3-2,6-(C_6H_5)$_2$ where all isopropyl groups are replaced with H atoms (see Table 5). It is remarkable to note that each of the bonding components changes by less than 1 kcal/mol. Thus, the direct electronic influence of the isopropyl groups on the

Table 5. NOCV[b] Contributions to ΔE_{orb}[a] for the Trans-Bent ArEEAr[c] Model Compounds Carried Out with the BP86 Functional

compound	$\Delta E_{orb}^{\pi^{y}}$ [a]	$\Delta E_{orb}^{\sigma*-\pi}$	$\Delta E_{orb}^{\sigma-\pi*}$	$\Delta E_{orb}^{\pi^{x}*}$	ΔE_{orb}^{rest}
Si[c]	−32.3	−36.7	−38.1		−8.9
Ge[c]	−33.1	−35.7	−35.6		−9.2
Sn[c]	−22.8	−19.5	−25.0		−7.6
Pb[c]				−44.7	−6.3

[a] $\Delta E_{orb} = \Delta E_{orb}^{\pi^{y}} + E_{orb}^{\sigma*-\pi} + \Delta E_{orb}^{\sigma-\pi*} + \Delta E_{orb}^{rest}$ for E = Si, Ge, and Sn. [b] Based on doublet fragments. [c] Ar = C_6H_3-2,6-(C_6H_5)$_2$. [d] Energies in kcal/mol.

E−E bond is minimal. There is some reduction in the stabilization ΔE_{rest}^{orb} as the isopropyl groups are replaced by H atoms. It represents the loss of hyperconjugation into the σ* orbitals on Pr^{i} induced by steric interactions. It is clear from the above discussion that the NOCV−ETS scheme can provide a detailed analysis of quite complex systems without having to make use of simplified models such as REER (R = H, Me). In fact, such models are unable to reveal the most important factors for the stability of the ArEEAr complexes, namely, the favorable dispersive interactions of the isopropyl groups on different E atoms. Further, the insight provided here suggests ways in which one might stabilize the lighter ArEEAr congeners by adding more isopropyl groups. However, such a strategy might somewhat be hampered by the steric constraints introduced by the shorter E−E distance.

We have also calculated the NOCV contributions to ΔE_{orb} for the model systems ArEEAr with Ar = C_6H_3-2,6-(C_6H_5)$_2$, where all isopropyl groups are replaced with H atoms (see Table 5). It is remarkable to note that each of the bonding components changes by less than 1 kcal/mol. Thus, the direct electronic influence of the isopropyl groups on the E−E bond is minimal. There is some reduction in the stabilization ΔE_{rest}^{orb} as the isopropyl groups are replaced by H atoms. It represents the loss of hyperconjugation into the σ* orbitals on Pr^{i} induced by steric interaction. It is clear from the above discussion that the NOCV−ETS scheme can provide a detailed analysis of quite complex systems without having to make use of simplified models such as REER (R = H, Me). In fact, such models are unable to reveal the most important factors for the stability of the ArEEAr complexes, namely, the steric and electronic properties of the isopropyl groups. Further, the insight provided here suggests ways in which one might stabilize the lighter ArEEAr congeners by adding more isopropyl groups. However, such a strategy might somewhat be hampered by the steric constraints introduced by the shorter E−E distance.

Also shown in Table 6 is NOCV analysis of trans-bent Ar′SiSiAr′ for LDA, BP86, B3LYP, and BHLYP. We note that ΔE_{orb} as well as the three major contributions $\Delta E_{orb}^{\pi^{y}}$, $\Delta E_{orb}^{\sigma-\pi*}$, and

Table 6. NOCV[c] Contributions[a] to ΔE_{orb}[b] for Trans-Bent Ar′SiSiAr Carried out with Different Functionals (Energies in kcal/mol)

functional	$\Delta E_{orb}^{\pi^{y}}$ [b]	$\Delta E_{orb}^{\sigma*-\pi}$	$\Delta E_{orb}^{\sigma-\pi*}$	ΔE_{orb}^{rest}
LDA	−35.6	−38.4	−39.8	−13.1
BP86	−32.4	−36.6	−38.2	−13.4
B3LYP	−33.1	−34.5	−35.9	−13.8
BHLYP	−49.5	−29.7	−21.4	−17.8

[a] See Figure 6. [b] $\Delta E_{orb} = \Delta E_{orb}^{\pi^{y}} + E_{orb}^{\sigma*-\pi} + \Delta E_{orb}^{\sigma-\pi*} + \Delta E_{orb}^{rest}$. [c] Based on doublet fragments.

dx.doi.org/10.1021/ic401149h | Inorg. Chem. 2013, 52, 8378−8388

$\Delta E_{orb}^{\sigma*-\pi}$ changes little on going from LDA to BP86 and B3LYP. For BHLYP, there are somewhat larger variations in the three contributing terms to ΔE_{orb}. However, ΔE_{orb} is the same for all four functionals within 4 kcal/mol. Thus, the large overbinding found for LDA is not associated with ΔE_{orb} but rather with ΔE_{Pauli}, as mentioned previously.

NOCV–ETS Analysis of the Factors Influencing the Trans-Bent Angle in ArEEAr. Tables 7 and 8 report the ETS analysis of the Si and Pb compounds, respectively, as a function of the C–E–E angle. It is clear from Table 8 that ΔE_{int} has a minimum close to the optimized angle at $\theta = 120°$. This angle is a compromise between $\Delta E_{orb} + \Delta E_{disp}$, which prefers a smaller angle, and ΔE_{steric}, for which angles larger than 120° are preferred. For E = Pb, we see the same trends. However, now the steric interaction is reduced because of the longer E–E distance. As a result, the equilibrium is close to $\theta = 90°$. The NOCV–ETS analysis provided in Tables 7 and 8 affords the first study of the factors determining the trans-bent conformation in the real systems. Previously, such studies have been limited to REER models with R = H and R. While REER compounds might be of interest in their own right, they are unable to simulate the actual steric and dispersive interactions found in ArEEAr. It is thus not surprising that REER realize conformations not observed by ArEEAr. Even in the trans-bent conformation, the E–E distances and θ angles in REER can differ considerably from those observed in ArEEAr, especially for E = Sn and Pb.[6,7] We supply in the Supporting Information a full NOCV–ETS analysis of Ar′EEAr′ [E = Si, Ge, Sn; Ar′ = C_6H_3-2,6-(C_6H_3-2,6-Pr^i_2)$_2$] and Ar*PbPbAr* [Ar* = C_6H_3-2,6-(C_6H_2-2,4,6-Pr^i_3)$_2$] in their linear conformations.

Table 7. ETS[d] Analysis for Ar′SiSiAr′ Where the Angle (θ) Ar′–Si–Si Is Varied (Energies in kcal/mol)

θ[c]	ΔE_{Pauli}	ΔE_{elstat}	ΔE_{steric}[a]	ΔE_{orb}	ΔE_{disp}	ΔE_{int}[b]
80	1296.4	−544.6	751.8	−474.8	−51.6	225.4
90	601.3	−254.3	347.0	−270.6	−48.0	28.4
100	304.9	−127.1	177.8	−184.5	−42.0	−48.6
110	197.7	−84.1	113.6	−153.1	−35.0	−74.5
120	171.7	−78.1	93.6	−144.8	−28.5	−79.7
130	141.9	−70.0	71.9	−123.3	−26.7	−78.0
140	199.1	−96.9	102.2	−151.0	−18.7	−67.5
150	222.6	−107.0	115.6	−156.7	−15.6	−56.7

[a]Steric interaction energy, $\Delta E_{steric} = \Delta E_{Pauli} + \Delta E_{elstat}$. [b]Total Interaction energy, $\Delta E_{int} = \Delta E_{steric} + \Delta E_{orb} + \Delta E_{disp}$. [c]$\theta$ in degrees. [d]Based on doublet fragments.

Table 8. ETS[d] Analysis for Ar*PbPbAr* Where the Angle (θ) Ar*–Pb–Pb Is Varied (Energies in kcal/mol)

θ[c]	ΔE_{Pauli}	ΔE_{elstat}	ΔE_{steric}[a]	ΔE_{orb}	ΔE_{disp}	ΔE_{int}[b]
80	265.5	−155.2	110.3	−99.0	−65.2	−53.9
90	140.2	−95.2	45.0	−76.4	−51.0	−82.3
100	108.6	−76.2	32.4	−66.9	−35.6	−70.2
110	98.6	−68.0	30.6	−59.7	−24.8	−53.8
120	93.1	−62.0	31.1	−57.0	−18.0	−43.9
130	87.6	−56.1	31.5	−52.0	−13.7	−34.2
140	81.2	−50.0	31.1	−45.6	−11.0	−25.5
150	74.3	−44.4	29.9	−38.7	−9.5	−18.3

[a]Steric interaction energy, $\Delta E_{steric} = \Delta E_{Pauli} + \Delta E_{elstat}$. [b]Total Interaction energy, $\Delta E_{int} = \Delta E_{steric} + \Delta E_{orb} + \Delta E_{disp}$. [c]$\theta$ in degrees. [d]Based on doublet fragments.

Singlet–Triplet Gap. We have so far assumed that all of our ArEEAr systems have a ground state that can be described as a closed-shell singlet. It follows from our analysis in Figure 4 that ArEEAr (E = Si, Ge, Sn) for such a singlet has the three occupied valence shells $(\sigma_{EE})^2(\sigma_{EE}*)^2(\pi^y_{EE})^2$ at highest energy and the empty shells $(\pi^x_{EE})^0(\pi^{y*}_{EE})^0$ at lowest energy, whereas ArPbPbAr has the configuration $(\sigma_{EE})^2(\sigma_{EE}*)^2(\pi^y_{EE})^2(\pi^x_{EE})^0(\pi^{y*}_{EE})^0$. The corresponding singlet closed-shell determinantal wave functions are in conventional DFT given by the KG determinantal $\Psi^S_1 = |\sigma_{EE}\overline{\sigma}_{EE}\sigma_{EE}*\overline{\sigma}_{EE}*\pi^y_{EE}\overline{\pi}^y_{EE}|$ for E = Si, Ge, and Sn and the corresponding KS determinant $\Psi^S_2 = |\sigma_{EE}\overline{\sigma}_{EE}\sigma_{EE}*\overline{\sigma}_{EE}*\pi^x_{EE}\overline{\pi}^x_{EE}|$ for E = Pb. Here the superscript "–" indicates an orbital of β spin. However, the possibility exists that one or more of the electron pairs are weakly coupled so that a high-spin triplet state with the valence configuration $(\sigma_{EE})^2(\sigma_{EE}*)^2(\pi^y_{EE})^1(\pi^x_{EE})^1(\pi^{y*}_{EE})^0$ is preferred. We have carried out calculations on the adiabatic triplet–singlet energy gap in order to investigate this possibility. The calculations were based on the SF-CV(2) scheme outlined in the Theory section with the triplet as a reference. Table 9 displays the calculated adiabatic gap for the four compounds with a trans-bent geometry using the LDA-VWN, BP86, BLYP, PBE, B3LYP, and BHLYP functionals. The estimated vertical gaps are slightly functional-dependent,[48−50] as was found in previous studies. The largest vertical singlet–triplet gaps in absolute terms were obtained for LDA, and the smallest were calculated for the hybrid functionals (B3LYP and BHLYP). All of the compounds revealed a negative gap for the trans-bent systems, which means that the singlet is of lower energy than the triplet. This is in agreement with previous theoretical studies on REER systems, including a spin-flip time-dependent DFT calculation (SF-TDDFT),[7] which is nearly identical with our SF-CV(2) procedure. Thus, the calculated gaps with B3LYP are −25.2 kcal/mol (Si), −22.4 kcal/mol (Ge), −18.2 kcal (Sn), and −6.0 kcal/mol (Pb) for the real system compared to −32.4 kcal/mol (Si), −27.6 kcal/mol (Ge), −2.0 kcal/mol (Sn), and −6.4 kcal/mol (Pb) for MeEEMe using the same functional. We attribute the substantial difference for E = Sn to the use[7] of a model system that differs in key geometrical parameters from those used in ArEEAr. Thus, the Sn–Sn distance in MeSnSnMe was 0.4 Å longer than that in ArSnSnAr.

Table 9. Singlet–Triplet Energy Gap (ΔE_{ST}) for the Four ArEEAr (E = Si, Ge, Sn, Pb) Compounds in Their Ground State Trans-Bent Geometry (Energy in eV)

	ΔE_{ST}[a]					
compound	LDA	BLYP	BP86	PBE	B3LYP	BHLYP
$Si_2Ar'_2$	−1.33	−1.22	−1.14	−1.18	−1.09	−1.01
$Ge_2Ar'_2$	−1.16	−1.10	−0.98	−1.03	−0.97	−0.90
$Sn_2Ar'_2$	−0.94	−0.90	−0.77	−0.83	−0.79	−0.74
Pb_2Ar*_2	−0.45	−0.50	−0.37	−0.40	−0.26	−0.29

[a]The negative sign indicates that the singlet state is of lower energy than the triplet state. All of the trans-bent compounds showed a singlet ground state.

Diradical Character. The fact that the spin-flip calculations revealed a singlet ground state does not necessary mean that all electrons are perfectly paired as in Ψ^S_1 or Ψ^S_2. The singlet could in full or in part be open shell with two electrons of opposite spins in different orbitals. In fact, SF-CV(2) (and SF-TDDFT)[7] is, in contrast to regular KS-DFT, able to describe a system as a mixture of open- and closed-shell singlets with a wave function for ArEEAr that is given by

dx.doi.org/10.1021/ic401149h | Inorg. Chem. 2013, 52, 8378–8388

$$\Psi^{S}_{SF} = C_1\Psi^{S}_{1} + C_2\Psi^{S}_{2} + C_3\Psi^{S}_{3} + \sum_{n_{SF}}^{N_{SF}} C_{n_{SF}}\Psi^{S}_{n_{SF}} \quad (19)$$

according to eq 10. In eq 19, $\Psi_1^S = |\sigma_{EE}\overline{\sigma}_{EE}\sigma_{EE}{}^*\overline{\sigma}_{EE}{}^*\pi^y_{EE}\overline{\pi}^y_{EE}|$ is generated from $\Psi_1^T = |\sigma_{EE}\overline{\sigma}_{EE}\sigma_{EE}{}^*\overline{\sigma}_{EE}{}^*\pi^y_{EE}\pi^x_{EE}|$ by the spin-flip substitution $\pi^x_{EE} \rightarrow \overline{\pi}^y_{EE}$, whereas $\Psi_2^S = |\sigma_{EE}\overline{\sigma}_{EE}\sigma_{EE}{}^*\overline{\sigma}_{EE}{}^*\pi^x_{EE}\overline{\pi}^x_{EE}|$ is obtained from Ψ_1^T by the spin-flip replacement $\pi^y_{EE} \rightarrow \overline{\pi}^x_{EE}$. Further, $\Psi_3^S = 1/\sqrt{2}\{|\sigma_{EE}\overline{\sigma}_{EE}\sigma_{EE}{}^*\overline{\sigma}_{EE}{}^*\pi^x_{EE}\overline{\pi}^y_{EE}| + |\sigma_{EE}\overline{\sigma}_{EE}\sigma_{EE}{}^*\overline{\sigma}_{EE}{}^*\overline{\pi}^x_{EE}\pi^y_{EE}|\}$ is reached from Ψ_1^T by the spin-flip transpositions $\pi^x_{EE} \rightarrow \overline{\pi}^x_{EE}$ and $\pi^y_{EE} \rightarrow \overline{\pi}^y_{EE}$. Finally, $\Psi^S_{n_{SF}}$ corresponds to one of the N_{SF} possible remaining spin-flip replacements generated by substituting one of the occupied orbitals of Ψ_1^T and $\Psi_{-1}^T = |\sigma_{EE}\overline{\sigma}_{EE}\sigma_{EE}{}^*\overline{\sigma}_{EE}{}^*\overline{\pi}^y_{EE}\overline{\pi}^x_{EE}|$ with one of the corresponding vacant orbitals of opposite spin. In eq 19, Ψ_1^S and Ψ_2^S represent the closed-shell singlet character of Ψ^S_{SF}, whereas Ψ_3^S and the sum over all $\Psi^S_{n_{SF}}$ represent the open-shell or diradical side of Ψ^S_{SF}. The weights of the contributing determinants are shown in Tables S4 and S5 in the Supporting Information. We find for E = Si, Ge, and Sn that the dominating contribution comes from C_1. For a given functional, the C_1 values differ little between elements, and for a given element, C_1 ranges from $C_1 = 0.99$ (LDA) to $C_1 = 0.93$ (BHLYP) (Tables S4 and S5 in the Supporting Information). The remaining part comes from many small $\Psi^S_{n_{SF}}$ contributions that represent the diradical nature. Thus, our analysis would indicate a diradical character of around 5% (or less) that is constant for all three elements E = Si, Ge, and Sn. For E = Pb, the dominating contribution is the closed-shell Ψ_2^S with $C_2 \approx 0.95$. Thus, for Pb, the maximum diradicaloid character is also 5%. That the percentage should be small seems reasonable in view of the triplet−singlet gap.

Jung et al.[7] pointed to eq 19 as a way in which to assess the degree of diradicaloid nature in the E−E bonds. Unfortunately, they did not report the different weights and used only SF-TDDFT to calculate the singlet−triplet splitting. The authors assessed instead the degree of diradical character from a natural orbital analysis based on ab initio complete-active-space SCF (CASSCF)[54] calculations. Such an analysis describes the electron configuration of REER (E = Si, Ge, Sn) with fractional occupations as $(\sigma_{EE})^2(\sigma_{EE}{}^*)^{2-\delta_1}\delta_1(\pi^y_{EE})^{2-\delta_2}(\pi^x_{EE})^{\delta_1}(\pi^{y*}_{EE})^{\delta_2}$ rather than $(\sigma_{EE})^2(\sigma_{EE}{}^*)^2(\pi^y_{EE})^2(\pi^x_{EE})^0(\pi^{y*}_{EE})^0$ for KS-DFT and HF. The fractional occupation numbers Δ_1 and Δ_2 are from qualitative considerations taken to mean that the degree of diradical character is $(\Delta_1 + \Delta_2) \times 10^2$%. In this way, the authors concluded that the diradical contribution was between 30−25% for E = Si, Ge, and Sn and 8% for E = Pb. For E = Si, Ge, and Sn, this would mean that the combined sum of squares of all weights $C^2_{n_{SF}}$ corresponding to $\Psi^S_{n_{SF}}$ for the spin-flip replacements $\sigma_{EE}{}^* \rightarrow \overline{\pi}^y_{EE}$, $\overline{\sigma}_{EE}{}^* \rightarrow \pi^y_{EE}$, $\pi^x_{EE} \rightarrow \overline{\pi}^{y*}_{EE}$, and $\overline{\pi}^x_{EE} \rightarrow \pi^{y*}_{EE}$ with respect to the triplet reference should be between 0.30 and 0.25. In our SF-CV(2)-DFT calculations, we find this contribution to be 2 orders of magnitude smaller and more in line with what one would expect in view of the large calculated singlet−triplet splitting. The diradical singlet components such as $\Psi^S_{n_{SF}}$ from the spin-flip replacements $\sigma_{EE}{}^* \rightarrow \overline{\pi}^y_{EE}$, $\overline{\sigma}_{EE}{}^* \rightarrow \pi^y_{EE}$, $\pi^x_{EE} \rightarrow \overline{\pi}^{y*}_{EE}$, and $\overline{\pi}^x_{EE} \rightarrow \pi^{y*}_{EE}$ appear as pure excited singlet states well above the first triplet.

V. CONCLUDING REMARKS

The present study is the first that has given a detailed analysis of the role played by isopropyl groups in stabilizing the E−E bond in ArEEAr (where E = Si, Ge, Sn, and Pb and Ar = terphenyl ligand). This analysis was carried out by employing the NOCV method together with the ETS scheme. In NOCV−ETS analysis, we consider ArEEAr as formed from two ArE fragments with a doublet ground-state configuration $\sigma^2\pi^1$. For E = Si, Ge, and Sn, it revealed one π bond perpendicular to the CEEC plane and two σ/π-type bonds in the plane, While similar bonding pictures have been obtained in previous model studies[6,7,9] with Ar = H and CH_3, the NOCV−ETS scheme was able to obtain quantitative estimates for the strength of the various σ/π components without artificial truncations of the system. Especially, it was shown that all three bonding components have the same strength. Thus, ArEEAr with E = Si, Ge, and Sn should be considered to have a triple bond. The ArPbPbAr system was found to have a single σ bond with a C−Pb−Pb trans-bent angle close to 90°. Such a crossover in bonding has been observed before[7,9] and rationalized as caused by an increasing stability of the doublet compared to the quartet in EAr. We point out that a contributing factor is a reduction of the out-of-plane bonding overlap in $\tilde{\pi}^y$ compared to $\tilde{\pi}^{x*}$ as the E−E bond distance increases (Figure 3).

As a completely new aspect, NOCV−ETS analysis was able to show that the electronic influence of the isopropyl substituents on the σ/π components differs little from that of H atoms. Rather, the stabilizing influence of the isopropyl substituents stems from dispersive van der Waals attractions between Pr^i groups on aryl rings attached to different E atoms as well as hyperconjugation involving donation into σ^* orbitals on Pr^i. The dispersive interaction amounts to −27.5 kcal/mol (Si), −29.1 kcal/mol (Ge), −26.2 kcal/mol (Sn), and −44.0 kcal/mol (Pb). The larger dispersive stabilization for Pb reflects the fact that the longer Pb−Pb and Pb−C bonds sterically allow for more isopropyl groups with Ar = C_6H_3-2,6-(C_6H_2-2,4,6-Pr^i_3)$_2$ compared to the other elements where Ar = C_6H_3-2,6-(C_6H_3-2,6-Pr^i_2)$_2$. Thus, in spite of the lower bond order, the E−E bond strength for E = Pb is stronger than that for the other elements because the weaker bonding interaction ΔE_{orb} is more than compensated for by a weaker steric repulsion and a more favorable dispersive attraction. NOCV−ETS analysis revealed that the observed trans-bent angles are a compromise between steric factors that favor larger angles and electronic factors ($\Delta E_{orb} + \Delta E_{disp}$) favoring smaller angles. The trans-bent angle θ has so far been studied by REER model systems (R = H, Me) where ΔE_{disp} is absent and ΔE_{steric} different. It is thus not surprising that the E−E distances and θ angles in REER can differ considerably from those observed in ArEEAr, especially for E = Sn and Pb.[7]

It is finally concluded from our quantitative SF-CV(2)-DFT calculations that the real ArEEAr systems reveal little if any diradical character of the E−E bond, in contrast to a previous qualitative analysis of model systems.

■ ASSOCIATED CONTENT

Supporting Information

NOCV−ETS and SF-CV(2)-DFT analysis of Ar′EEAr′ [E = Si, Ge, Sn; Ar′ = C_6H_3-2,6-(C_6H_3-2,6-Pr^i_2)$_2$] and Ar*PbPbAr* [Ar* = C_6H_3-2,6-(C_6H_2-2,4,6-Pr^i_3)$_2$] in their linear conformations. This material is available free of charge via the Internet at http://pubs.acs.org.

■ AUTHOR INFORMATION

Corresponding Author

*E-mail: ziegler@ucalgary.ca.

dx.doi.org/10.1021/ic401149h | Inorg. Chem. 2013, 52, 8378−8388

Notes

The authors declare no competing financial interest.

■ ACKNOWLEDGMENTS

This work was supported by the NSERC. The computational resources of WESTGRID were used for all calculations. T.Z. thanks the Canadian Government for a Canadian Research Chair. I.S. is grateful to Dr. Masood Parvez for access to the CCDC.

■ REFERENCES

(1) Pu, L.; Twamley, B.; Power, P. P. *J. Am. Chem. Soc.* **2000**, *122*, 3524.
(2) Stender, M.; Phillips, A. D.; Wright, R. J.; Power, P. P. *Angew. Chem., Int. Ed.* **2002**, *41*, 1785.
(3) Cui, C.; Brynda, M.; Olmstead, M. M.; Power, P. P. *J. Am. Chem. Soc.* **2004**, *126*, 6510.
(4) Cui, C.; Olmstead, M. M.; Power, P. P. *J. Am. Chem. Soc.* **2004**, *126*, 5062.
(5) (a) Stender, M.; Phillips, A. D.; Power, P. P. *Chem. Commun. (Cambridge)* **2002**, 1312. (b) Phillips, A. D.; Wright, R. J.; Olmstead, M. M.; Power, P. P. *J. Am. Chem. Soc.* **2002**, *124*, 5930.
(6) Landis, C. R.; Weinhold, F. *J. Am. Chem. Soc.* **2006**, *128*, 7335.
(7) Jung, Y.; Brynda, M.; Power, P. P.; Head-Gordon, M. *J. Am. Chem. Soc.* **2006**, *128*, 7185.
(8) Power, P. P. *Nature* **2010**, *463*, 171.
(9) Chen, Y.; Hartmann, M.; Diedenhofen, M.; Frenking, G. *Angew. Chem., Int. Ed.* **2001**, *40*, 2052.
(10) Lein, M.; Krapp, A.; Frenking, G. *J. Am. Chem. Soc.* **2005**, *127*, 6290.
(11) Lischka, H.; Kohler, H. *J. Am. Chem. Soc.* **1983**, *105*, 6646.
(12) Colegrove, B. T.; Schaefer, H. F. *J. Am. Chem. Soc.* **1991**, *113*, 1557.
(13) Bogey, M.; Bolvin, H.; Demuynck, C.; Destombes, J.-L. *Phys. Rev. Lett.* **1991**, *66*, 413.
(14) (a) Tranquier, G.; Malrieu, J.-P. *J. Am. Chem. Soc.* **1987**, *109*, 5303. (b) Carter, E. A.; Goddard, W. A. *J. Phys. Chem.* **1986**, *90*, 998.
(15) Han, Y.-K.; Bae, C.; Lee, Y. S.; Lee, S. Y. *J. Comput. Chem.* **1998**, *19*, 1526.
(16) Grev, R. S.; Deleeuw, B. J.; Schaefer, H. F., III. *Chem. Phys. Lett.* **1990**, *165*, 257.
(17) Palagyi, Z.; Schaefer, H. F., III; Kapuy, E. *J. Am. Chem. Soc.* **1993**, *115*, 6901.
(18) Malcolm, N. O. J.; Gillespie, R. J.; Popelier, P. L. A. *J. Chem. Soc., Dalton Trans.* **2002**, 3333.
(19) Allen, T. L.; Fink, W. H.; Power, P. P. *J. Chem. Soc., Dalton Trans.* **2000**, 407.
(20) Sekiguchi, A.; Zigler, S. S.; West, R.; Michl, J. *J. Am. Chem. Soc.* **1986**, *108*, 4241.
(21) Yamaguchi, Y.; Deleeuw, B. J.; Richards, C. A.; Schaefer, H. F.; Frenking, G. *J. Am. Chem. Soc.* **1994**, *116*, 11922.
(22) Snyder, L C.; Wasserman, Z. R.; Moskowitz, J. W. *Int. J. Quantum Chem.* **1982**, *21*, 565.
(23) Binkley, J. S. *J. Am. Chem. Soc.* **1984**, *106*, 603.
(24) Luke, B. T.; Pople, J. A.; Krogh-Jespersen, M. B.; Apeloig, Y.; Karni, M.; Chandrasekhar, J.; Schleyer, P. v. R. *J. Am. Chem. Soc.* **1986**, *108*, 270.
(25) Lischka, H.; Koehler, H. J. *J. Am. Chem. Soc.* **1983**, *105*, 6646.
(26) Wiberg, N.; Niedermeyer, W.; Fischer, G.; Noth, H.; Suter, M. *Eur. J. Inorg. Chem.* **2002**, 1066.
(27) Wiberg, N.; Vasisht, S. K.; Fischer, G.; Mayer, P. *Z. Allg. Anorg. Chem.* **2004**, *630*, 1823.
(28) Sekiguchi, A.; Kinjo, R.; Ichinohe, M. *Science* **2004**, *305*, 1755.
(29) (a) Nagase, S.; Kobayashi, K.; Takagi, N. *J. Organomet. Chem.* **2000**, *611*, 264. (b) Takagi, N.; Nagase, S. *Organometallics* **2001**, *20*, 5498. (c) Zhu, Z.; Fischer, R. C.; Ellis, B. D.; Rivard, E.; Merrill, W. A.; Olmstead, M. M.; Power, P. P.; Guo, J. D.; Nagase, S.; Pu, L. *Chem.—Eur. J.* **2009**, *15*, 5263.
(30) Ziegler, T.; Rauk, A. *Inorg. Chem.* **1979**, *18*, 1755.
(31) Ziegler, T.; Rauk, A. *Inorg. Chem.* **1979**, *18*, 1558.
(32) Ziegler, T.; Rauk, A. *Theor. Chim. Acta* **1977**, *46*, 1.
(33) Michalak, A.; Mitoraj, M.; Ziegler, T. *J. Phys. Chem. A* **2008**, *112*, 1933.
(34) Mitoraj, M.; Michalak, A.; Ziegler, T. *J. Chem. Theory Comput.* **2009**, *5*, 962.
(35) Grimme, S.; Ehrlich, S.; Goerigk, L. *J. Comput. Chem.* **2011**, *32*, 1456.
(36) Ziegler, T.; Seth, M.; Krykunov, M.; Autschbach, J.; Wang, F. *J. Chem. Phys.* **2009**, *130*, 154102.
(37) Koch, W.; Holthausen, M. C. *A Chemist's Guide to Density Functional Theory*; Wiley-VCH: New York, 2001.
(38) Wang, F.; Ziegler, T. *J. Chem. Phys.* **2004**, *121*, 12191.
(39) Wang, F.; Ziegler, T. *J. Chem. Phys.* **2005**, *122*, 074109.
(40) Wang, F.; Ziegler, T. *Int. J. Quantum Chem.* **2006**, *106*, 2545.
(41) Zhekova, H. R.; Seth, M.; Ziegler, T. *J. Chem. Theor. Comput.* **2011**, *7*, 1858.
(42) Zhekova, H.; Seth, M.; Ziegler, T. *J. Chem. Phys.* **2011**, *135*, 184105.
(43) Seidu, I.; Zhekova, H. R.; Seth, M.; Ziegler, T. *J. Phys. Chem. A* **2012**, *116*, 2268.
(44) te Velde, G.; Bickelhaupt, F. M.; Baerends, E. J.; van Gisbergen, S. J. A.; Fonseca Guerra, C.; Snijders, J. G.; Ziegler, T. *J. Comput. Chem.* **2001**, *22*, 931.
(45) Vosko, S. H.; Wilk, L.; Nusair, M. *Can. J. Phys.* **1980**, *58*, 1200.
(46) Becke, A. D. *Phys. Rev. A* **1988**, *38*, 3098.
(47) Perdew, J. P.; Wang, Y. *Phys. Rev. B* **1986**, *33*, 8822.
(48) Lee, C.; Yang, W.; Parr, R. G. *Phys. Rev. B* **1988**, *37*, 785.
(49) Perdew, J. P.; Burke, K.; Ernzerhof, M. *Phys. Rev. Lett.* **1996**, *77*, 3865.
(50) Becke, A. D. *J. Chem. Phys.* **1993**, *98*, 1372−1377.
(51) van Lenthe, E.; Baerends, E. J.; Snijders, J. G. *J. Chem. Phys.* **1993**, *99*, 4597.
(52) van Lenthe, E.; Baerends, E. J.; Snijders, J . G. *J. Chem. Phys.* **1994**, *101*, 9783.
(53) Schwarz, W. H. E.; Schmidbaur, H. *Chem.—Eur. J.* **2012**, *18*, 4470.
(54) Siegbahn, P. E. M.; Almlöf, J.; Heiberg, A.; Roos, B. O. *J. Chem. Phys.* **1981**, *74*, 2384.